Electrical Power and Energy Systems 153 (2023) 109281

Contents lists available at ScienceDirect

International Journal of Electrical Power and Energy Systems

journal homepage: www.elsevier.com/locate/ijepes

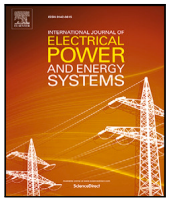

Short communication

Analysis of equilibrium points and optimal grid support of grid-forming modular multilevel converter for balanced and unbalanced faults

Daniel Westerman Spier *, Carlos Collados-Rodriguez, Eduardo Prieto-Araujo, Oriol Gomis-Bellmunt

Centre d'Innovació Tecnològica en Convertidors Estàtics i Accionaments (CITCEA), Departament d'Enginyeria Elèctrica, Universitat Politècnica de Catalunya (UPC), ETSEIB Av. Diagonal 647, Barcelona, 08028, Spain

ARTICLE INFO

Keywords:
Grid-forming
Modular multilevel converter
Voltage support
Current limitation

ABSTRACT

This short-communication presents a steady-state analysis of a grid-forming Modular Multilevel Converter (MMC) providing optimal voltage support to the AC network under normal and constrained conditions. The analysis is performed based on a multi-objective function (OF) optimization problem which prioritizes to maximize the positive-sequence and to minimize the negative- and zero-sequence voltage components at the point of common coupling (PCC) while it also considers the minimization of the arm impedance losses, respectively. If the voltage condition at the PCC is satisfied, the optimization attempts to reduce the arm impedance losses; otherwise, the algorithm prioritizes the PCC's voltage components in order to minimize the error. Different network voltage and internal fault scenarios are evaluated, where it is shown that the suggested problem formulation can be used to obtain the optimal MMC's quantities, providing voltage support during the faults.

1. Introduction

The Modular Multilevel Converter (MMC) has become the most attractive type of Voltage Source Converter (VSC) to be used in High Voltage Direct Current (HVDC) transmission systems [1]. In HVDC applications, the MMC has been mostly applied as a grid-following converter where AC currents are provided to the network and aligned with the AC network voltage based on the phase-angle reference given by a phase-locked loop (PLL) [2]. However, as more renewable energy generation is integrated with the power system, the MMC is starting to perform a new role as a grid-forming converter (GFOR) [3]. Under this operation (such as offshore wind farms, interconnection of asynchronous power systems and islanded grids), the converter must be regulated in order to keep the voltage magnitude at the point of common coupling (PCC) equals to $U = 1$ pu with a specified angle θ [4], as shown in Fig. 1.

Although there are several publications regarding the model and analysis of the MMC, only few authors have investigated the converter operating as GFOR under fault scenarios [4–6]. The main difference between grid-following (GFOL) and GFOR operating modes relies in the fact that in GFOL mode the converter behaves as a current source, injecting/absorbing active and reactive currents to provide voltage/frequency support to the network [7]. Whereas in GFOR mode, the MMC operates as a voltage source, regulating the magnitude and phase-angle of the PCC voltage. Consequently, when regulated in GFOR mode, the MMC must keep the voltage at the PCC balanced and with magnitude as close as possible to 1 pu. In addition, the MMC must also maintain its quantities within their design limitations.

However, to the best of the authors knowledge, a generalized control agnostic optimization-based reference calculation algorithm for MMCs' operating in GFOR mode capable of providing optimal grid support while considering the converters design limitations, has not been proposed yet. Aiming to cope with such challenges, this short communication brings the following contributions:

- Formulation of an optimization-based reference calculation for MMCs operated in GFOR mode to ensure the maximum positive-sequence voltage and minimal negative- and zero-sequence voltage components at the PCC.
- The optimization problem can be modified for different prioritizations, e.g. maximize the mitigation of negative-sequence component (attempting to balance the PCC voltage), based on the grid-code requirements.
- The proposed optimization considers the arms' and AC current and voltage limits as well as the SM capacitor voltage maximum and minimum voltage (to avoid overmodulation).

* Corresponding author.
E-mail address: daniel.westerman@upc.edu (D.W. Spier).

https://doi.org/10.1016/j.ijepes.2023.109281
Received 16 September 2022; Received in revised form 27 January 2023; Accepted 27 May 2023
Available online 14 June 2023

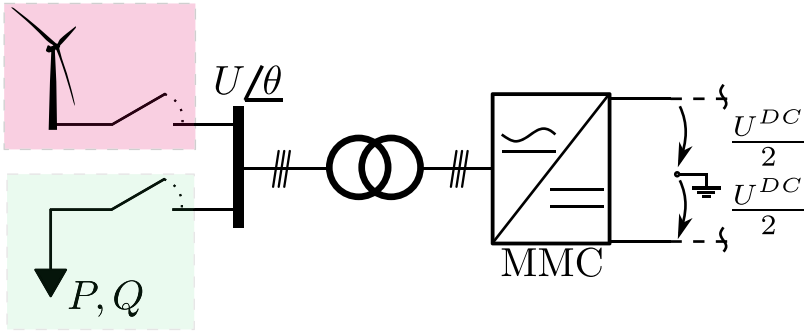

Fig. 1. MMC connection as grid-forming converter.

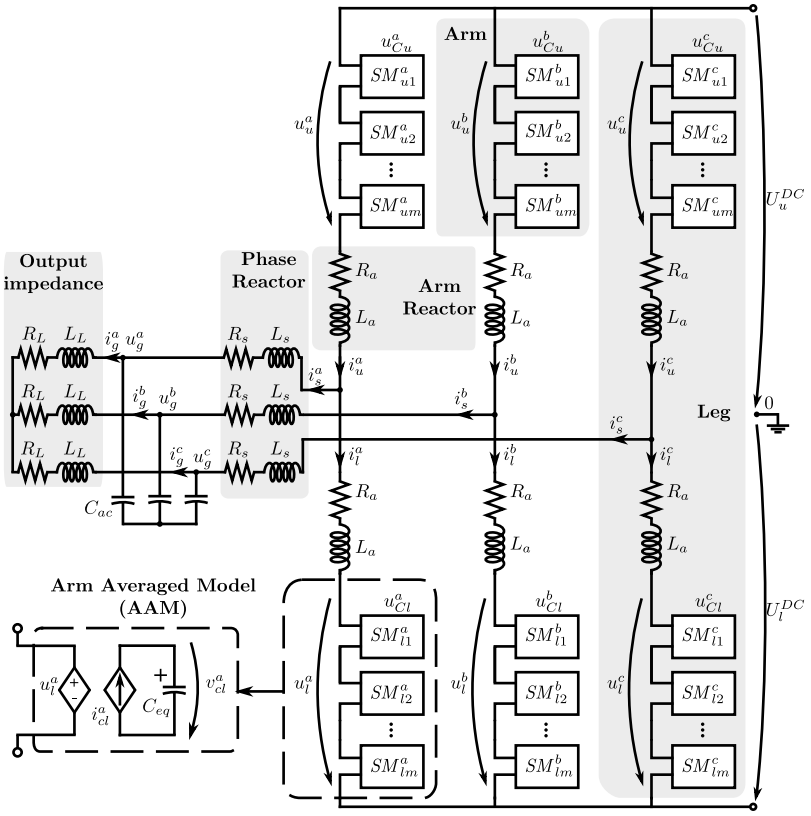

Fig. 2. Scheme of the MMC as grid-forming converter.

- Different SM topologies can be considered, based on the SM voltage limits.

This short-communication considers that the MMC is operated as GFOR supplying a passive load that is used to emulate different faults in the PCC, as shown in Fig. 2. In addition, different AC and DC unbalanced voltage and internal fault scenarios are simulated in order to show the suggested optimization model performance. To validate the proposed analysis, the output values of the optimization are compared with an average model of the MMC in time-domain simulations for all the different case studies.

2. Optimal analysis of MMCs in GFOR operations

This section describes the control agnostic optimization problem for MMC operating as GFOR to provide grid voltage support. The multi-objective problem is an adaptation of the grid-following optimization problem proposed in [7], and it allows the prioritization among the positive-, negative- and zero-sequence voltage components at the PCC and the minimization of the arm impedance losses.[1] Furthermore, the optimization-based reference calculation algorithm assumes that a cascaded control might be employed to regulate the converter. As the voltage control action can be ease by assuming a plant in its design stage, the voltage measurements consider a capacitor impedance (which can either be from the transmission system line or a physical one) [3].

2.1. Description of the optimization problem

The optimal analysis is developed considering the phasor notation $\underline{X}^k = X_r^k + jX_i^k = X^k\angle\theta^k$, with $x(t) = X^k\text{Re}\{e^{j(\omega t+\theta^k)}\}\ \forall k \in (a,b,c)$. In this study, the load or source connected to the GFOR converter is modeled as a constant impedance. It can be noted that a PQ node could

[1] Note that for GFOL applications, the objective function would be modified in order to prioritize the injection/absorption of active and reactive currents to comply with the grid code requirements.

be considered by defining the equivalent impedance at nominal voltage condition using $\underline{Z}_L^k = U_g^{k^2} / \left(P^k - jQ^k\right)$.[2]

The main goal is to keep the PCC positive-sequence voltage as close as to 1 pu, the negative- and zero-sequence components to 0, throughout the operation of the converter while maintaining the MMC's quantities within their design limits. The OF, linear and non-linear equality constraints and the non-linear inequality constraints are described as ($k \in (a,b,c)$)

$$\underset{\substack{\underline{I}_{u,l}^k, I_{u,l}^{kDC}, \underline{I}_s^k, \underline{I}_g^k, \\ \underline{U}_{u,l}^k, U_{u,l}^{kDC}, \underline{U}_{n0}, \underline{U}^{+-0}}}{\text{minimize}} \quad \begin{aligned} &-\lambda_p U_g^+ + \lambda_n U_g^- + \lambda_z U_g^0 + \\ &\lambda_l \left(R_a \sum_{k=a}^{c} \left(I_u^{k^2} + I_l^{k^2} + I_u^{kDC^2} + I_l^{kDC^2} \right) \right) \end{aligned} \tag{1a}$$

subject to

$$\underline{U}_{0n} = \underline{U}_g^k + \underline{Z}_s(\underline{I}_u^k - \underline{I}_l^k) + \underline{Z}_a \underline{I}_u^k + \underline{U}_u^k \tag{1b}$$

$$\underline{U}_{0n} = \underline{U}_g^k + \underline{Z}_s(\underline{I}_u^k - \underline{I}_l^k) - \underline{Z}_a \underline{I}_l^k - \underline{U}_l^k \tag{1c}$$

$$\underline{I}_s^k = \underline{I}_u^k - \underline{I}_l^k \tag{1d}$$

$$2\underline{I}_s^k \left(\underline{Z}_L^k + \underline{Z}_s\right) = -\underline{U}_u^k + \underline{U}_l^k \tag{1e}$$

$$0 = \underline{I}_s^a + \underline{I}_s^b + \underline{I}_s^c \tag{1f}$$

$$0 = \underline{I}_u^a + \underline{I}_u^b + \underline{I}_u^c \tag{1g}$$

$$I_g^k = \underline{I}_s^k - \underline{U}_g^k / \underline{Z}_{C_{ac}} \tag{1h}$$

$$0 = \underline{I}_g^a + \underline{I}_g^b + \underline{I}_g^c \tag{1i}$$

$$U_u^{DC} + U_l^{DC} = U_u^{kDC} + U_l^{kDC} + R_a \left(I_u^{kDC} + I_l^{kDC}\right) \tag{1j}$$

$$0 = I_u^{kDC} - I_l^{kDC} \tag{1k}$$

$$I_{tot}^{DC} = I_u^{aDC} + I_u^{bDC} + I_u^{cDC} \tag{1l}$$

$$2\left(U_u^{aDC} - U_l^{aDC}\right) = \left(U_u^{bDC} - U_l^{bDC} + U_u^{cDC} - U_l^{cDC}\right) \tag{1m}$$

$$0 = \left(U_u^{bDC} - U_l^{bDC} - U_u^{cDC} + U_l^{cDC}\right) \tag{1n}$$

$$P_{u\to l}^k = \text{Re}\left\{\underline{U}_u^k \underline{I}_u^k - \underline{U}_l^k \underline{I}_l^k\right\} \tag{1o}$$

$$P_{a\to b} = \text{Re}\left\{\left(\underline{U}_u^a \underline{I}_u^a + \underline{U}_l^a \underline{I}_l^a\right) - \left(\underline{U}_u^b \underline{I}_u^b + \underline{U}_l^b \underline{I}_l^b\right)\right\} \tag{1p}$$

$$P_{a\to c} = \text{Re}\left\{\left(\underline{U}_u^a \underline{I}_u^a + \underline{U}_l^a \underline{I}_l^a\right) - \left(\underline{U}_u^c \underline{I}_u^c + \underline{U}_l^c \underline{I}_l^c\right)\right\} \tag{1q}$$

$$0 = \sum_{k=a}^{c} \left[\text{Re}\left\{\underline{U}_u^k \underline{I}_u^k + \underline{U}_l^k \underline{I}_l^k\right\} + U_u^{kDC} I_u^{kDC} + U_l^{kDC} I_l^{kDC}\right] \tag{1r}$$

$$U_g \leqslant U_{max}^{AC} \tag{1s}$$

$$I_s^k \leqslant I_{max}^{AC} \tag{1t}$$

$$I_{u,l}^k + I_{u,l}^{kDC} \leqslant I_{max}^{arm} \tag{1u}$$

$$U_{Cu,l_{max}}^k \leqslant U_{C_{max}} \tag{1v}$$

$$0 \leqslant U_{u,l}^k + U_{u,l}^{kDC} \leqslant U_{Cu,l_{min}}^k \tag{1w}$$

where, $\underline{Z}_L^k$ is the output impedance of phase k which can be modified in order to emulate different faults in the PCC, $\underline{Z}_s$ is the phase reactor impedance, the arm impedance is given as $\underline{Z}_a$ and $\underline{Z}_{C_{ac}}$ is the filter impedance.[3] The OF, given in (1a), consists of four terms with different priorities in which three of them are used to regulate the PCC's voltage and one is employed minimize the arm impedance losses. The priorities used in this short-communication are set as $\lambda_p \gg \lambda_n \gg \lambda_z \gg \lambda_l$. Eqs. (1b)–(1i) describe the AC current and voltage relations, whereas (1j)–(1n) are the DC current and voltage equalities. The amount of power transfer between the upper and lower arms of the converter as well as among the phase-legs of the MMC is regulated through (1o)–(1q) based on the inputs ($P_{u\to l}^k$, $P_{a\to b}$ and $P_{a\to c}$. Under normal operations, these values are equal to zero. However, during transients, they might present variations that must be regulated to avoid tripping the converter's protection system. In this analysis, such power difference values are set to be equal to 0. Expression (1r) ensures that the sum of the average AC power in all the converter's arms is equal to the sum of the DC power; thus, steady-state conditions are achieved. Finally, (1s)–(1w) limits the PCC's voltage (1s), the currents flowing through the AC-side and arms (1t)–(1u), the maximum allowed voltage in the equivalent arm capacitors (1v), and the maximum and minimum voltages to be applied in the arms of the converter (1w). Note that, the sub-modules (SMs) are based on half-bridge structures; thus their minimum allowed value is equal to 0. If different SM technology was considered (e.g. full-bridge), negative voltages could be applied into the converter's arms. The methodology employed to obtained expressions (1v) and (1w) is discussed in [7].

2.2. Implementation of the optimization algorithm in real-time applications

The suggested optimization-based reference calculation for MMCs operating in GFOR mode can be potentially integrated with the different converter's controllers in two manners. The first approach assumes that the optimization is executed offline (see Fig. 3a). The multiple MMC's reference outputs for the distinct operating points simulated offline are stored as a data table in the processor's memory. Thus, depending on the system's conditions, the device can interpolate the desired reference to be sent to the controller's value based on the stored data. Although such approach can be used with the non-linear optimization algorithm, it might lead to errors depending on the size of the data-table (limited by the memory available in the processor).

The second method would be to run the optimization in an online manner, as shown in Fig. 3b. Under this control method, the algorithm receives the HVDC system data and calculate the optimal references to be used by the MMC's regulators in real-time. Nevertheless, the proposed optimization problem in this paper is highly non-linear, leading to high computational burden. To cope with this issue, linearization techniques could be implemented in order to reduce the computational burden as done in [8] for GFOL applications.

3. Results

This section presents the results obtained when the proposed optimization algorithm is employed to calculate the references for grid-forming MMCs operating under different fault and constrained scenarios. The results obtained with the optimization are applied to an average model of the MMC and its time-domain responses are compared to validate the optimization problem and to confirm that the MMC's limitations are respected. The parameters used for the different cases studies are given in Table 1, based on the MMC-HVDC interconnection between Spain and France [9]. The desired reference voltage level in per-unit at the PCC is equal to $\underline{U}_g = 1\underline{/0°}$ pu.

3.1. Case study A: Unbalanced AC-side voltage sag

In this case study, the fault impedances $\underline{Z}_L^k$ are emulating a type C fault with $V = 0.1$ pu [10] by assuming $\underline{Z}_L^a = 1.0467\underline{/6.009°}$ pu and $\underline{Z}_L^b = \underline{Z}_L^c = 0.2696\underline{/6.009°}$ pu. The PCC voltages resultant from the optimization algorithm are equal to $\underline{U}_g^+ = 0.469\underline{/-1.263°}$ pu, $\underline{U}_g^- = 0.186\underline{/-1.263°}$ pu and $\underline{U}_g^0 = 0$. Such unbalanced behavior is due to the higher prioritization of the positive-sequence component over the negative-sequence one. As it can be in Fig. 4, the optimization is unable to provide extra voltage to the PCC as the AC grid currents for phases b and c are already achieving their maximum magnitude. Higher voltage levels in the PCC would cause such phase currents to exceed their allowed values, which may damage the transformer. Furthermore, it can also be noted that the optimization response (continuous line) is in close agreement with the converter response (dashed line) confirming the applicability of the optimal steady-state model.

[2] Note that negative resistance would be obtained for the generation source case.

[3] For RL filters, the same optimization formulation could be used. The main difference is that the negative term in (1h) would be equal to zero.

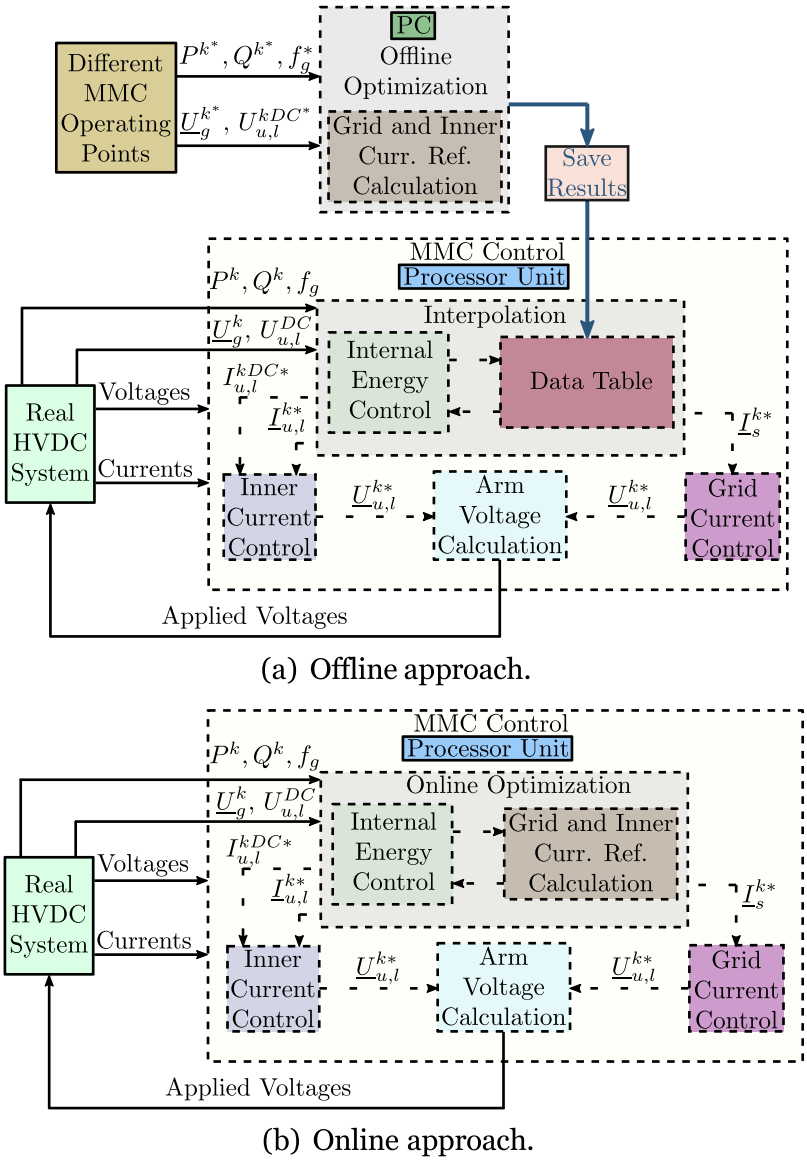

Fig. 3. Potential implementation of the proposed optimization-based reference calculation with the converter's controller in real-time.

Table 1
System parameters for the online optimization.

Parameter	Symbol	Value	Units
Rated power	S	1000	MVA
Rated power factor	$\cos\phi$	0.95 (c)	–
Rated AC-side voltage (line-line RMS)	U_g	325	kV
HVDC link voltage	U^{DC}	±320	kV
Phase reactor impedance	$\underline{Z}_s$	0.005 + j 0.18	pu
Arm reactor impedance	$\underline{Z}_{arm}$	0.01 + j 0.15	pu
Converter modules per arm	$N^k_{u,l_{arm}}$	433	–
Sub-module capacitance	C_{SM}	9.5	mF
Optimal weighting factors 1	λ_p	1	–
Optimal weighting factor 2	λ_n	10^{-2}	–
Optimal weighting factor 3	λ_z	10^{-3}	–
Optimal weighting factor 4	λ_l	10^{-5}	–
Maximum MMC arm current	I^{arm}_{max}	1.1	pu
Maximum AC grid current	I^{AC}_{max}	1.1	pu
Maximum equivalent's arm cap. voltage	$U^k_{C_{u,l_{max}}}$	1.2	pu
Minimum equivalent's arm cap. voltage	$U^k_{C_{u,l_{min}}}$	0.8	pu

3.2. Case study B: HVDC voltage unbalance

For this case study, it is considered that AC side of the converter is operated under normal conditions with $\underline{Z}^a_L = \underline{Z}^b_L = \underline{Z}^c_L = 1.0467\angle 6.009°$ pu and with an active power exchange of 1 pu. For the HVDC side, the upper pole is also operated without any contingency whereas the voltage level of the lower HVDC pole suffers a voltage drop (from 320 kV to 220 kV). As it can be seem in Fig. 5, the AC side and arm currents are not reaching their limits. However, due to the characteristics of the fault and considering the sub-modules structures, the arms' applied voltages achieve their minimum allowed value. Due to the voltage limitation caused by the DC pole unbalance, the PCC voltage cannot reach 1 pu, being equal to $\underline{U}^+_g = 0.955\angle 0°$ pu and $\underline{U}^-_g = \underline{U}^0_g = 0$.

3.3. Case study C: Saturation in the MMC's arm voltage

The goal of this case study is to analyze and confirm that the optimization algorithm is capable to operate under arm constrained conditions. To do so, it has been considered that the number of available SMs in the lower arm of phase a has been reduced from 433 to 350. Although such condition in real applications might be extreme, the results show that the proposed optimization algorithm can converge in a

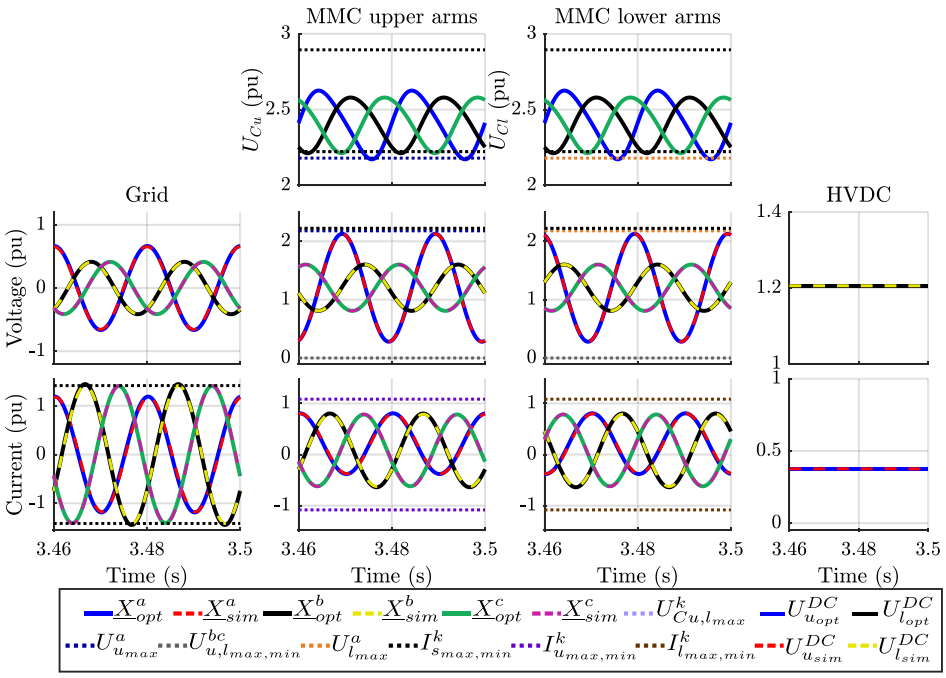

Fig. 4. Time-domain comparison for an unbalanced voltage sag type C.

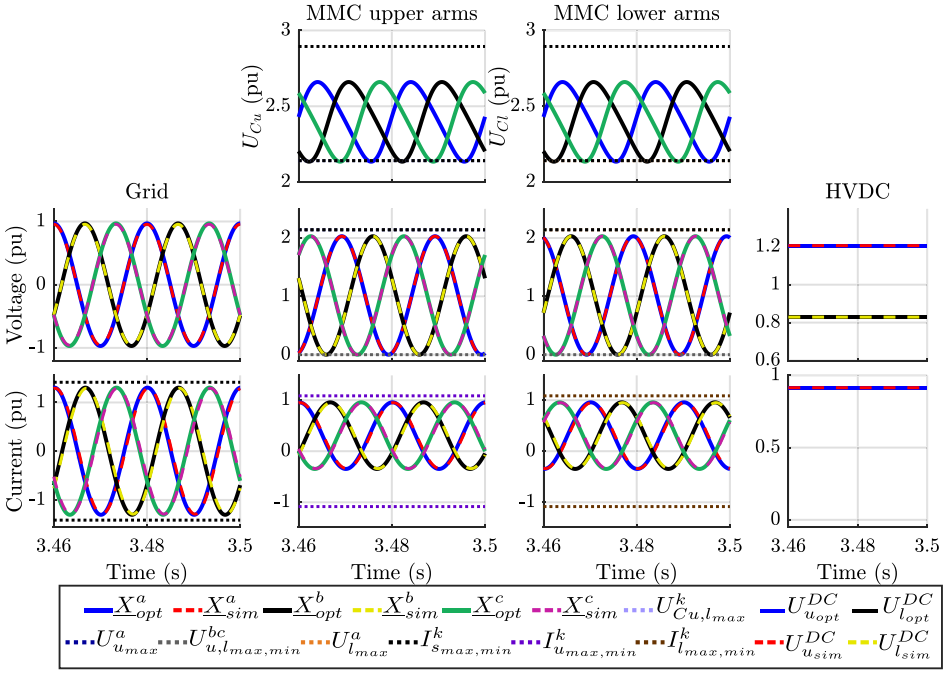

Fig. 5. Time-domain waveforms for an HVDC unbalanced voltage condition with U_u^{DC} = 320 kV and U_l^{DC} = 220 kV.

solution that can maintain the MMC operating even in such constrained scenario. As it can be observed in Fig. 6, the output voltage for phase *a* suffers the biggest reduction as it is the phase directly affected by such condition. Furthermore, since the optimization attempts to achieve values as close as possible to unsaturated values, it increases the voltage levels in the upper and lower arms of phases *b* and *c*. However, in order to avoid overmodulations, these voltage levels cannot exceed the values equal to their respective minimum equivalent arm capacitor voltage. Although there is a 20% reduction in the number of available SMs, the algorithm is capable of synthesize reasonable positive-sequence voltage with relatively low negative-sequence voltage levels. Finally, the PCC voltage levels under such event are equal to $\underline{U}_g^+ = 0.742\underline{/2.344°}$ pu, $\underline{U}_g^- = 0.215\underline{/-177.65°}$ pu and $\underline{U}_g^0 = 0$.

3.4. Case studies summary

In Fig. 7, the PCC voltage phasors in the *abc* frame for the different case studies are depicted. In case study A, the grid-forming voltages present unbalanced characteristics, in which the magnitude of the voltages is more affected than the phase-angle displacement among the phases. For case B, the PCC voltages present a balanced profile. As the fault occurs in phase *a* for case study C, the voltage level of this phase is

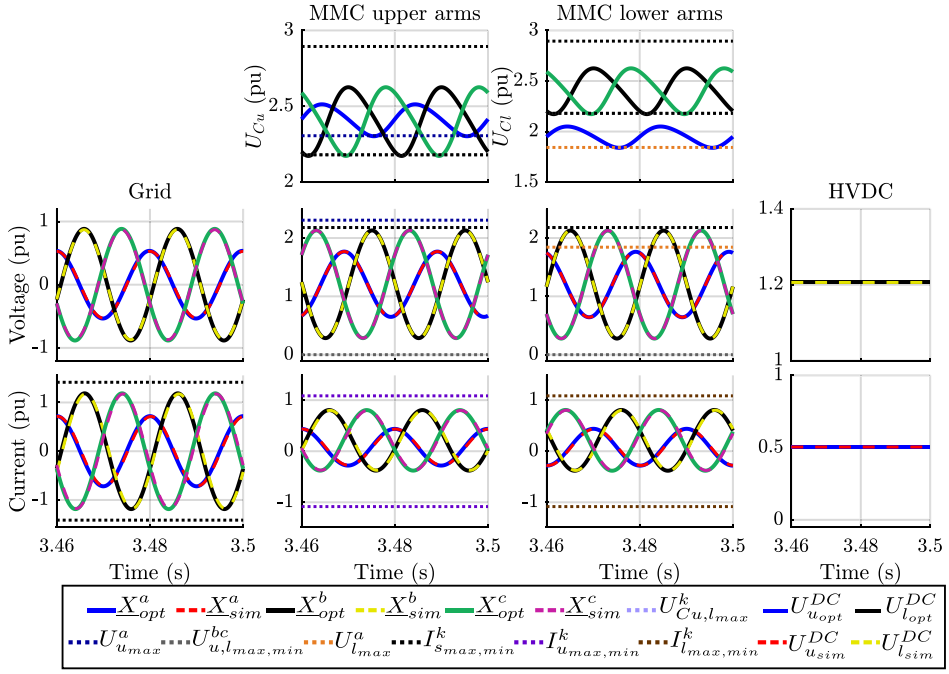

Fig. 6. Time-domain waveforms considering an unbalanced number of available arms in the MMC with $N^a_{l_{arm}} = 350$, $N^a_{u_{arm}} = 433$ and $N^{b,c}_{u,l_{arm}} = 433$.

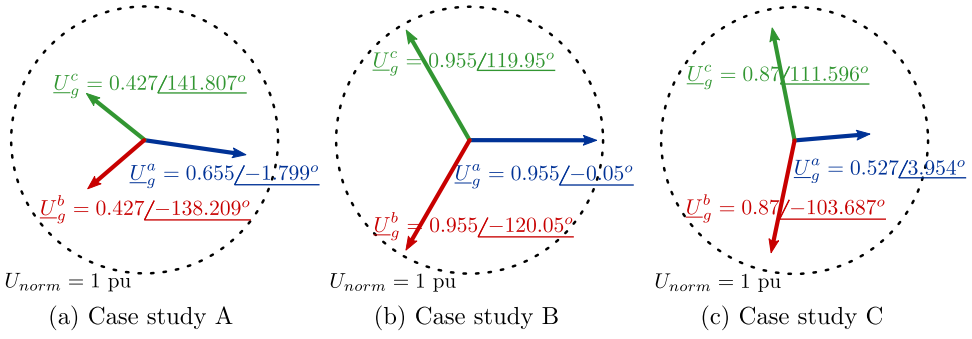

Fig. 7. PCC voltage phasors for the different case studies analyzed.

the one with the highest reduction in comparison to the other phases b and c. Finally, the PCC voltage has unbalanced characteristics as some internal quantities of the converter have achieved their limitation (see case study C).

4. Conclusion

In this short-communication, an equilibrium analysis of a GFOR MMC providing optimal voltage support to the network under unbalanced network voltage conditions and internal faulted scenarios is presented. The multi-objective algorithm prioritizes to maximize the positive-sequence voltage at the PCC while minimizing the remaining voltage components, as well as, the arm impedance losses. To validate the suggested model, time-domain simulations comparing the model's and the converter's responses during different AC and DC unbalanced network voltage and constrained conditions are performed. In addition, the results indicate that the suggested optimal steady-state model can be potentially used to obtain the converter's references. Finally, based on this initial study, linearization techniques can be employed in future work in order to integrate such algorithm with the different controllers of the MMC to be solved in real-time.

CRediT authorship contribution statement

Daniel Westerman Spier: Conceptualization, Methodology, Writing, Validation. **Carlos Collados-Rodriguez:** Conceptualization, Review and editing. **Eduardo Prieto-Araujo:** Conceptualization, Supervision. **Oriol Gomis-Bellmunt:** Conceptualization, Supervision.

Declaration of competing interest

The authors declare that they have no known competing financial interests or personal relationships that could have appeared to influence the work reported in this paper.

Data availability

No data was used for the research described in the article.

Acknowledgments

This work was supported by the Ministerio de Ciencia e Innovación (Proyecto Equired) under Grant PID2021-124292OB-I00. This work was also supported by the Agencia Estatal De Investigación,

Spain under Grant PID2021-127788OA-I00. Eduardo Prieto-Araujo is an associate professor of the Serra Húnter programme. The work of Oriol Gomis-Bellmunt was also supported by the Institució Catalana de Recerca i Estudis Avançats (ICREA), Spain Academia Program.

References

[1] Van Hertem D, Gomis-Bellmunt O, Liang J. HVDC grids: for offshore and supergrid of the future. IEEE press series on power engineering, Wiley; 2016.
[2] Westerman Spier D, Prieto-Araujo E, López-Mestre J, Gomis-Bellmunt O. Improved current reference calculation for MMCs internal energy balancing control. IEEE Trans Power Deliv 2022;37(3):1488–501.
[3] Sánchez-Sánchez E, Prieto-Araujo E, Gomis-Bellmunt O. The role of the internal energy in MMCs operating in grid-forming mode. IEEE Trans Emerg Sel Top Power Electron 2020;8:949–62.
[4] Schönleber K, Prieto-Araujo E, Ratés-Palau S, Gomis-Bellmunt O. Extended current limitation for unbalanced faults in MMC-HVDC-connected wind power plants. IEEE Trans Power Deliv 2018;33:1875–84.
[5] Freytes J, Li J, de Préville G, Thouvenin M. Grid-forming control with current limitation for MMC under unbalanced fault ride-through. IEEE Trans Power Deliv 2021;36:1914–6.
[6] Mahr F, Jaeger J. Advanced grid-forming control of HVDC systems for reliable grid restoration. In: 2018 IEEE power energy soc. gen. meet.. PESGM, 2018, p. 1–5.
[7] Westerman Spier D, Prieto-Araujo E, López-Mestre J, Gomis-Bellmunt O. Optimal current reference calculation for MMCs considering converter limitations. IEEE Trans Power Deliv 2021;36(4):2097–108.
[8] Westerman Spier D, Rodriguez-Bernuz J-M, Prieto-Araujo E, López-Mestre J, Junyent-Ferré A, Gomis-Bellmunt O. Real-time optimization-based reference calculation integrated control for MMCs considering converter limitations. IEEE Trans Power Deliv 2022;37(4):2886–901.
[9] Abdel-Moamen MA, Shaaban SA, Jurado F. France-Spain HVDC transmission system with hybrid modular multilevel converter and alternate-arm converter. In: 2017 innovations in power and advanced computing technologies (I-PACT). 2017, p. 1–6.
[10] Bollen M, Zhang L. Different methods for classification of three-phase unbalanced voltage dips due to faults. Electr Power Syst Res 2003;66:59–69.